

FORESEE: Multimodal and Multi-view Representation Learning for Robust Prediction of Cancer Survival

Liangrui Pan¹, Yijun Peng¹, Yan Li¹, Yiyi Liang², Liwen Xu¹, Qingchun Liang³, Shaoliang Peng¹

¹Hunan University ²Shanghai Jiaotong University ³Central South University

{panlr, pengyijun,s2310w1062,xuliwen, slpeng}@hnu.edu.cn, liangyiyi@renji.com, 503079@csu.edu.cn

Abstract

Integrating the different data modalities of cancer patients can significantly improve the predictive performance of patient survival. However, most existing methods ignore the simultaneous utilization of rich semantic features at different scales in pathology images. When collecting multimodal data and extracting features, there is a likelihood of encountering intra-modality missing data, introducing noise into the multimodal data. To address these challenges, this paper proposes a new end-to-end framework, FORESEE, for robustly predicting patient survival by mining multimodal information. Specifically, the cross-fusion transformer effectively utilizes features at the cellular level, tissue level, and tumor heterogeneity level to correlate prognosis through a cross-scale feature cross-fusion method. This enhances the ability of pathological image feature representation. Secondly, the hybrid attention encoder (HAE) uses the denoising contextual attention module to obtain the contextual relationship features and local detail features of the molecular data. HAE's channel attention module obtains global features of molecular data. Furthermore, to address the issue of missing information within modalities, we propose an asymmetrically masked triplet masked autoencoder to reconstruct lost information within modalities. Extensive experiments demonstrate the superiority of our method over state-of-the-art methods on four benchmark datasets in both complete and missing settings.

1 Introduction

With the popularity of third-generation high-throughput sequencing, the cost for doctors to obtain pathological images and molecular data has decreased and the efficiency has been much more accessible [Liao *et al.*, 2023]. Illustrated in Figure 1, pathological images can offer semantic information at both cellular and tissue levels at different magnifications. Molecular data includes cancer-related ribonucleic acid (RNA), copy number variation (CNV), and mutation (MUT) data. Due to the rapid advancement of artificial

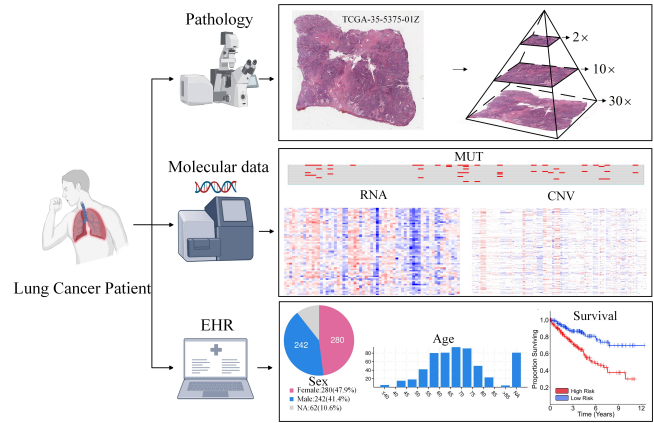


Figure 1: Obtaining graphical representations of multimodal data (Pathology, Molecular data, and EHR) from lung cancer patients.

intelligence, deep learning methods utilizing multimodal data are extensively applied in predicting patient survival. Certain technologies, such as AttnMIL [Chen *et al.*, 2022], GSCNN [Mobadersany *et al.*, 2018], Pathomic [Chen *et al.*, 2020], that incorporate feature fusion are proved to be successful in predicting patient survival. However, this method ignores modal incompleteness. It solely enhances feature representation in a unimodal and then employs straightforward feature fusion techniques like vector splicing [Mobadersany *et al.*, 2018], modal data aggregation [Cheerla and Gevaert, 2019], Kronecker product [Chen *et al.*, 2020] to handle multimodal data. As these methods do not thoroughly discuss the missing modality and the missing information within the modality, the predictive performance of the model will be unreliable in practical applications.

The methods based on multimodal data have indeed significantly improved the accuracy of multimodal cancer survival prediction. Unfortunately, these methods neglected the issue of incomplete data in real-life scenarios, arising from patients neglecting certain examinations or being unwilling to conduct them. Hence, the development of a robust model capable of effectively addressing unforeseen missing data in predicting patient survival is essential [Wang *et al.*, 2022]. This alleviates the burden on both physicians and patients. Due to certain constraints, prior methods such as

linear interpolation [Zhang *et al.*, 2017], matrix factorization [Zhang and Wu, 2022], and generative adversarial networks [Kaneko and Harada, 2020] face challenges when applied to the multimodal survival prediction of cancer patients. In summary, all challenges can be summarized as follows: 1) the heterogeneity and huge dimensional changes of medical multimodal data (e.g., WSI, molecular data) complicate data understanding and processing. Importantly, all methods in survival prediction ignore the simultaneous use of rich semantic features at different scales in WSI. 2) When collecting, organizing and feature extracting multi-modal data, missing modal data and missing data within a modality are prone to occur. 3) Multimodal data obtained through advanced instruments in diverse detection environments inevitably introduce noise [Krebschull and Zador, 2015].

In this paper, we propose a novel end-to-end multimodal framework for robustly predicting patient survival, named FORESEE. To address the heterogeneity of multimodal data and fully mine multimodal features related to prognosis, FORESEE proposes two strategies for extracting information from WSI and molecular data. Firstly, we segment WSI into patches at varying magnification levels and employ a graph structure to characterize multi-scale histopathology data. The cross-fusion transformer (CFT) learns contextual relationships across patches through a cross-scale feature cross-fusion method. This enhances the representation of histopathology images across various scales. Secondly, the novel hybrid attention encoder (HAE) uses a new contextual attention (CTA) module to capture the contextual features of molecular data and extract local feature details. Furthermore, the channel attention (CNA) module in HAE extracts global features of molecular data and improves the overall representation ability of molecular data. The wavelet transform module in HAE resolves the noise present in molecular data. Finally, to tackle the problem of missing intra-modal information, we introduce an asymmetric triplet masked autoencoder (TriMAE) with a non-uniform masks in FORESEE. Specifically, we simulate scenarios with missing data within various modalities. The encoder extracts features exclusively from visible features, while a lightweight decoder reconstructs multimodal data features using latent feature representations and masked tokens. The attention mechanism in the decoder enhances the local details of the reconstructed features.

Our contributions can be summarized as follows: 1) Based on the spatial topological graph structure of WSI, CFT in FORESEE can effectively cross-fuse features at the cellular level, tissue level, and tumor heterogeneity level. It leverages cross-scale contextual information to enhance the accuracy of survival predictions. 2) The novel HAE utilizes a new contextual attention module and a new channel attention module to learn features of molecular data, reducing the impact of noise in modal data. 3) The asymmetrically masked TriMAE is designed to reconstruct multimodal data features from latent feature representations and masked tokens. 4) End-to-end FORESEE has been extensively and experimentally validated on four cancer datasets of TCGA, achieving the state-of-the-art results and verifying the effectiveness of the above proposed solutions and methods.

2 Related Work

In recent years, with the continuous emergence of medical big data, clinicians have gradually improved cancer patient survival predictions beyond relying solely on clinical covariates and experience. Computational pathology, nuclear medicine, and third-generation sequencing technologies have made clinicians realize the importance of utilizing artificial intelligence to process multimodal data for supporting cancer survival predictions. In order to further enhance the accuracy of AI-based cancer patient survival prediction, some studies attempt to combine medical imaging data, genomics, and clinical records, proposing research on patient survival prediction based on multimodal data. Currently, most efforts in multimodal survival prediction are primarily focused on feature extraction and data fusion of modality data. Feature extraction from multimodal data commonly uses graph to construct spatial topological structures for image and text data representations. In this context, graph nodes represent feature information, and graph edges signify relationships between node features. For instance, MulGT utilizes a graph transformer architecture to extract low-level representations from graphs [Zhao *et al.*, 2023]. HEAT describes WSI as heterogeneous graphs and designs a novel pseudo-label-based semantic-consistent pooling mechanism to obtain graph-level features [Chan *et al.*, 2023]. Similarly, MG-Trans employs a patch anchored module (PAM) with multi-head self-attention (MSA) to generate class attention maps for identifying and sampling informative patches [Shi *et al.*, 2023]. Subsequently, multimodal data fusion primarily focuses on late fusion methods, such as Multimodal graph neural network (MGNN) [Gao *et al.*, 2020], GPDBN [Wang *et al.*, 2021], and Pathomics [Chen *et al.*, 2020]. Finally, early fusion methods worth mentioning include the Multimodal co-attention transformer (MCAT) [Chen *et al.*, 2021]. These methods effectively improve the accuracy of cancer patient survival predictions.

3 Methodology

3.1 Overview

Illustrated in Figure 2, CFT in FORESEE uses a cross-scale feature cross-fusion method to capture different scale feature representations and cross-scale contextual relationships in WSI. To the best of our knowledge, CFT is applied for survival prediction for the first time. HAE extracts local and global information from preprocessed molecular data. TriMAE performs masking operations on different modality data, leveraging feature, mask, and location information to recover potentially lost feature representations. The reconstructed multimodal features are blended and used for final survival prediction.

3.2 Multimodal Data Preprocessing

To meet the data requirements for predicting patient survival with multimodal data, we selected diagnostic pathology (P) data, RNA (R), CNV and MUT ($C\&M$) data from TCGA to constitute our multimodal data set $D = \{P, R, C\&M\}$.

Illustrated in Figure 2, WSI predominantly capture cell-level details at low magnification, shifting to tissue-level and

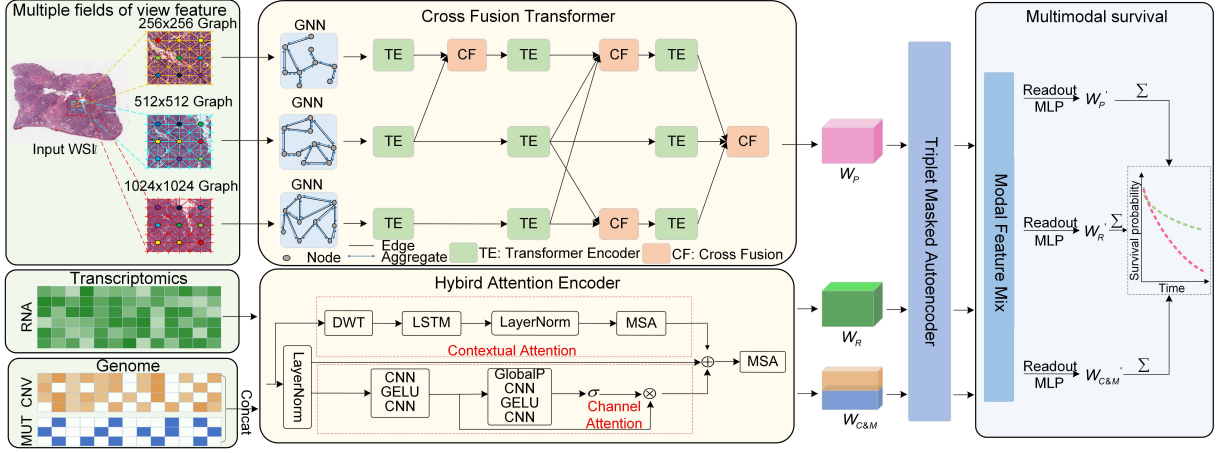


Figure 2: Flowchart depicting multimodal patient survival prediction. The flow chart comprises the multi-view feature extraction , CFT, HAE, TriMAE, and multimodal prediction survival module. Notably, GlobalP denotes the Global Pooling layer, and GELU serves as the activation function.

tumor heterogeneity level information when observed at high magnification. Therefore, we use a sliding window strategy to segment the WSI into patches of 256×256 , 512×512 , and 1024×1024 , representing small, medium, and large fields of view, respectively. Background is then removed, retaining patches containing image information. To reduce hardware requirements, patch embedding representations need to be extracted before model training. In this work, we use the KimiaNet [Riasatian *et al.*, 2021] to extract patch feature embeddings. Each patch embedding obtained is standardized into a 1024-dimensional vector. Connecting these vectorized feature representations in an 8-neighboring manner yields the graphical representation of pathology images at different scales, denoted as $G_P = \{V, E\}$. where V and E represent the sets of points and edges in the graph, respectively. The post-processed features of WSI are denoted as G_{P_s} , G_{P_m} and G_{P_l} . An adjacency matrix A defines the similarity between graph nodes. Secondly, the concat function is employed to merge $C\&M$ data, forming a unified modality. The aforementioned preprocessing involves P data and molecular data, constructing multimodal data consisting of P , R , and $C\&M$ for each patient.

3.3 Cross Fusion Transformer

The preprocessed field of view graph $G_P = \{V, E\}$ is a spatial topological diagram of all images in the field of view constructed from a set of nodes $V = \{v_1, v_2, \dots, v_o\}$ and the edges E between these nodes. Suppose $(v_m, v_n) \in E$ represents an edge from node $v_m \in V$ to $v_n \in V$, $N(v_m) = \{v_n \in V | (v_m, v_n) \in E\}$ represents the domain of node v_m , and $\bar{N}(v_m)$ represents $N(v_m) \cup \{v_m\}$. The graph G_P we designed is undirected, that is, $v_n \in N(v_m) \Leftrightarrow v_m \in N(v_n)$. Suppose $N(S) = \{v \in V | (v_m, v_n)\}$ represents the domain of node set S , and $\bar{N}(S)$ represents $N(S) \cup S$. Suppose $x_m \in R^{d_m}$ represents the characteristics of node v_m with dimension d_x . $h_m \in R^d$ is represented as the d -dimensional embedding of node v_m . Let $X = (x_1, x_2, \dots, x_n) \in R^{d_x \times n}$ and $H = (h_1, h_2, \dots, h_n) \in R^{d \times n}$. We use $H_S = (h_{m_k})_{k=1}^{|S|} R^{d \times |S|}$

to represent the embedding of the node set $S = (v_{m_k})_{k=1}^{|S|}$. $\bar{A} \in R^{p \times q}$ is a vectorized representation of a $p \times q$ matrix $A \in R^{p \times q}$, where $A_{m,n} \in A_{m+(n-1)p}$. Let A_n denote the n -th column of A . For positive integers L , $[L] = \{1, 2, \dots, L\}$. GNN updates the node's embedding L by minimizing the objective function. We first use GNN within $L = 2$ layer graph convolution to perform feature extraction on G_{P_s} , G_{P_m} and G_{P_l} to generate the final node embedding $H = H^L$, such as:

$$H^l = f_{W^l}(H^{l-1}; G_P), l \in [L], \quad (1)$$

When $H^0 = G_P$, f_{W^l} is the l -th layer feature transfer function of the learnable parameter W^l . f_{W^l} strictly follow the node aggregation and update method. The process is:

$$\begin{aligned} h_m^l &= u_{W^l}(h_m^{l-1}, F_{N(v_m)}^{l-1}, x_m); \\ F_{N(v_i)}^{l-1} &= \oplus_{W^l}(\{p_{W^l}(h_n^{l-1}) | v_n \in N(v_m)\}), l \in [L] \end{aligned} \quad (2)$$

Among them, p_{W^l} can generate a separate feature for each neighbor of v_m in the l -th feature transfer iteration. \oplus_{W^l} is an aggregation function that maps a set of features to the final feature $F_{N(v_m)}^{l-1}$. u_{W^l} is the feature h_m^{l-1} that is embedded using previous nodes, mapping post feature $F_{N(v_m)}^{l-1}$ and input feature x_m are used to update the optimization function of node embedding. Briefly, we use graph sampling and aggregation in CFT. The channel of each node is mapped to the hidden dimension, which is set to 500. The use of GNN establishes mutual communication between nodes in the feature map G_P under each field of view. Then, it saves the extracted features into $G_{P'}$ and passes it to the transformer encoder.

Each transformer learns representative features through a MSA mechanism. The transformer encoder comprises a MSA layer, LayerNorm (LN) layer, and feed-forward network (FFN) layer. Initially, the transformer encoder uses a MSA mechanism to extract abundant semantic information

from G_P' , denoted as G_P'' . To prevent gradient vanishing and enhance model performance, a residual connection is established to transfer information and fuse features G_P' and G_P'' . Subsequently, the LN layer is employed to standardize the output, and the FFN executes a non-linear transformation on complex semantic features to capture intricate patterns and features in the input data. To enhance the representation of semantic information and spatial relationships within these modules using CFT, we employ two transformer encoders to learn features for different fields of view.

To uncover cross-scale contextual correlations among distinct regions in histopathology images corresponding to different fields of view, we propose to use two types of cross-fusion schemes to blend features from different fields of view. In CFT, the first cross-fusion scheme combine G_{P_s}'' with G_{P_m}'' , G_{P_m}'' with G_{P_l}'' , while the second cross-fusion scheme integrates features from large, medium, and small fields of view. Illustrated in Figure 2, to facilitate the transformer encoder in learning cross-scale context correlations, remapping one-dimensional features $G_{P_l}'' \in R^{N^s \times D}$ and $G_{P_m}'' \in R^{N^s \times D}$ is necessary, followed by their integration into a shared feature space denoted as $G_{P_{l+m}}'' \in R^{(N^s+N^s) \times D}$. To achieve this objective, the reshaping function $R(\cdot)$ is employed to convert one-dimensional feature maps G_{P_l}'' and G_{P_m}'' into two-dimensional feature maps, followed by splicing operations. Subsequently, two-dimensional convolution is applied for multi-channel attention nonlinear mapping on the spliced features, leading to their fusion. The fused features undergo the upsampling operation of the CNN to maintain consistency between the output and input features. Subsequently, the cross-fusion features are fed into the channel global average pooling and fully connected layers to optimize the output results. Additionally, to avoid potential information loss during intersection, we apply weighting to the sum of the fused features and nonlinear mapping features, ensuring comprehensive integration of semantic information from both large and medium fields of view. The process involves:

$$F_G = Fusion(R(G_{P_l}'') \oplus R(G_{P_m}'')) \oplus R(G_{P_l}'') \oplus R(G_{P_m}'') \quad (3)$$

\oplus represents the operation of feature splicing, and $Fusion(\cdot)$ denotes the function of fusing features from both large and small fields of view. F_G corresponds to the output of feature fusion. Subsequently, the two-dimensional fused features undergo nonlinear transformation, mapping them to a one-dimensional feature space. Additionally, the features G_{P_m}'' and G_{P_s}'' undergo cross-fusion. The initial type of cross-fusion module is also applicable for the fusion of features G_{P_m}'' and G_{P_s}'' . To consolidate features from all fields of view, the second type of cross-fusion aims to intermix $F_{G_{P_l}}, F_{G_{P_m}}$, and $F_{G_{P_s}}$ processed by the second-layer transformer. The process of the second cross-fusion scheme is similar to the first one, and its process is $Fusion(R(F_{G_{P_l}}) \oplus R(F_{G_{P_m}}) \oplus R(F_{G_{P_s}})) \oplus R(F_{G_{P_l}}) \oplus R(F_{G_{P_m}}) \oplus R(F_{G_{P_s}})$.

3.4 Hybrid Attention Encoder

Given the presence of considerable noise in P , R , and $C\&M$ data, we employ discrete wavelet transform (DWT) in the CAT module to denoise this data. In DWT, we utilize the Daubechies (dbN) wavelets for preprocessing the input molecular data. Daubechies wavelets, being a class of compactly supported wavelet bases, are suitable for handling signals with mutation characteristics, effectively addressing some gene expression changes or mutated genes in genomic data [Adewusi and Al-Bedoor, 2001]. Through low-pass filter and high-pass filter, the signal is decomposed into approximation coefficients and detail coefficients at different scales (or frequencies).

The unit function is denoted by $u(t)$. Soft thresholding is applied to the detail coefficients after the wavelet transform, thereby eliminating noise. The wavelet coefficients after soft thresholding are then subjected to the inverse wavelet transform to reconstruct the denoised signal. For feature extraction from molecular sequencing data, LSTM [Huang *et al.*, 2015] has a significant advantage in handling and capturing long-term dependencies in R and $C\&M$ data. In LSTM, the input data at each time step is transformed into a fixed-length vector, representing the extracted features. Meanwhile, to obtain local attention features of molecular data, we propose using a self-attention mechanism to extract these features.

CNA introduces global information from molecular data to calculate the weight of CNA. The attention mechanism can use global information to weight features and activate more features. Illustrated in Figure 2, to reduce the computational cost associated with using a fixed-width convolution directly, we compress the number of channels the two convolutional layers to a constant, denoted as β . The output channels after the first convolution are compressed to $C\beta$, where C is the channel number of the first convolution. Then, the second convolution expands the features to C channels, followed by the adaptive adjustment of channel features using CNA. Finally, MSA is employed from feature extraction on the merged features. The workflow of the entire mixed attention encoder is as follows:

$$x_{CAT} = MSA(LN(LSTM(DWT(LN(x_{R||C\&M})))))) \quad (4)$$

$$x_{CNA} = \alpha CNA(LN(x_{R||C\&M})) \quad (5)$$

$$x_{HAE} = MSA(LN(x_{R||C\&M}) + x_{CAT} + x_{CNA}) \quad (6)$$

3.5 Triplet Masked Autoencoder

To ensure that the model is not adversely affected by missing features during inference, we designed a TriMAE to reconstruct the missing feature information in multimodal data. Inspired by SiamMAE [Gupta *et al.*, 2023], which can reconstruct detailed features of masked frames within videos. Through the analysis of multimodal data and features, we found that different modalities have missing features. Therefore, we propose a masking strategy in TriMAE, where each branch masks only one modality feature during the processing of multimodal data. The masking rate is set to be over 80%, making it challenging for features to reconstruct the

masked pixels through surrounding features. This compels the encoder to learn meaningful features.

TriMAE consists of an asymmetric encoder-decoder architecture. The encoder is based on three parallel transformers serving as the backbone network, operating only on unmasked feature patches. This significantly reduces the inference cost of the encoder. The decoder is a lightweight module composed of cross-attention layers and self-attention layers. The feature information obtained by encoders from different branches is focused on each other through a cross-attention layer and then complements missing information by mutually attending to each other through a self-attention layer. The input primarily comprises unmasked feature patches and masked tokens, where the masked features are shared and learned vectors for all missing positions. As illustrated in Figure 3, TriMAE takes features with masked information from different modalities as input and, through the learning process of the encoder and decoder, reconstructs missing feature details using contextual relationships and semantic information. TriMAE employs the attention mechanism principles of cross-attention layers to perform local attention calculations on reconstructed features from the three branches. After the feature cross calculation, further self-attention feature learning is applied to the reconstructed features to obtain the optimal feature representations for each modality data.

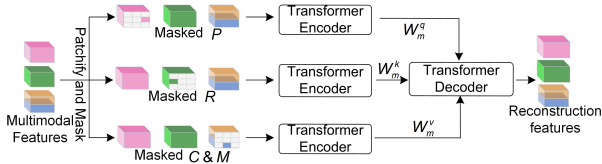


Figure 3: Flowchart for TriMAE to reconstruct missing data in multimodal data.

3.6 Training and Inference Strategies

To establish interaction among multimodal data, we designed a modal feature fusion module to mix information from different modalities and edge information of channels to promote comprehensive interaction between multimodal data. This process is represented as follows:

$$F = MLP(LN(MLP(x) + x) + x) \quad (7)$$

Finally, the survival output of modality m can be calculated as:

$$W_m = MLP(Readout(F_m)) \quad (8)$$

Therefore, the Cox loss of modality m can be defined as:

$$L_{Cox}^m = \sum_{i=1}^B \delta_i \left(-O_m(i) + \log \sum_{j:t_j > t_i} \exp(O_m(j)) \right) \quad (9)$$

Where $O_m(i)$ and $O_m(j)$ represent the survival outputs for the i -th and j -th patients in modality m , respectively. In summary, the loss for the entire model can be defined as:

$$L_{all}^m = \sum_{m \in M} \lambda_m L_{Cox}^m + \lambda_0 L_{TriMAE} \quad (10)$$

Where λ_0 and λ_m are adjustable parameters. Considering the complexity of multimodal, λ_0 and λ_m are set to five and one, respectively.

4 Experiment

4.1 Experimental Settings

Datasets. Diagnostic WSI and corresponding molecular and clinical data were collected from 2479 patients across BLCA, BRCA, LUAD and UCEC cancer datasets at TCGA through the NIH Genomic Data Commons Data Portal. The availability of CNVs, MUTs and RNA-Seq abundances for each WSI match. All molecular and clinical data were obtained from cBioPortal’s [Cerami *et al.*, 2012] quality control files.

Evaluation Metrics. This experiment employs the C-index and Kaplan-Meier (KM) analysis method to assess the performance and prediction accuracy of the survival analysis model [Xu and Chen, 2023].

Implementation. All experiments are based on NVIDIA GeForce RTX 4090. For the cancer datasets, we perform 5-fold cross-validation and report the cross-validated concordance index (C-Index) and its standard deviation (std). All models are developed using Python 3.9 based on the PyTorch 1.13.1 platform. After extensive experiments, we set some optimal hyper-parameters for the model. We adopt Adam optimizer with initial learning rate of 5×10^{-3} and weight decay of 1×10^{-5} , batch size set 50, epoch set 50, and Dropout set 0.2.

4.2 Comparison With State-of-the-Art Methods

We compare FORESEE with unimodal and multimodal state-of-the-art (SOTA) methods: for unimodal data, we adopt **DeepAttnMISL** [Yao *et al.*, 2020], **CLAM-SB** [Lu *et al.*, 2021], **CLAM-MB** [Lu *et al.*, 2021], **TransMIL** [Shao *et al.*, 2021], **DTFD-MIL** [Zhang *et al.*, 2022], **Cox** [Matsuo *et al.*, 2019], **SNNTrans** [Shao *et al.*, 2021], **XGBLC** [Ma *et al.*, 2022]. For multimodal data, we adopted **GSCNN** [Mobadersany *et al.*, 2018], **Pathomic** [Chen *et al.*, 2020], **Metric learning** [Cheerla and Gevaert, 2019], **MultiSurv** [Vale-Silva and Rohr, 2021], **MCAT** [Chen *et al.*, 2021], **HGCN** [Hou *et al.*, 2023], **MOTCat** [Xu and Chen, 2023], **AttnMIL** [Chen *et al.*, 2022], **SNN** [Chen *et al.*, 2022], **MMF** [Chen *et al.*, 2022], **Porpoise** [Chen *et al.*, 2022]. The results are shown in Table 1. Since different experiments use different cancer data sets, we restore the method in the article and re-experiment and obtain survival prediction results.

Unimodal v.s. Multimodal: FORESEE achieves the SOTA results in the BLCA, BRCA, and UCEC cancer datasets. This indicates that multimodal approaches can effectively enhance the accuracy of survival prediction, and FORESEE exhibits generalization. Furthermore, results based on the R modality generally outperform those based on the P modality. This is because genes determine phenotypes, and phenotypes are strongly associated with survival. However, XGBLC attains the SOTA result on the LUAD dataset. This suggests that the simple feature concatenation fusion method in FORESEE faces significant challenges on the LUAD dataset.

Methods	P	R	$C\&M$	BLCA	BRCA	LUAD	UCEC
DeepAttnMISL [Yao <i>et al.</i> , 2020]	✓			0.504±0.042	0.524±0.043	0.548±0.050	0.597±0.059
CLAM-SB [Lu <i>et al.</i> , 2021]	✓			0.559±0.034	0.573±0.044	0.594±0.063	0.644±0.061
CLAM-MB [Lu <i>et al.</i> , 2021]	✓			0.565±0.027	0.578±0.032	0.582±0.072	0.609±0.082
Trans-MIL [Shao <i>et al.</i> , 2021]	✓			0.575±0.034	0.666±0.029	0.642±0.047	0.655±0.046
DTFD-MIL [Zhang <i>et al.</i> , 2022]	✓			0.546±0.021	0.609±0.059	0.585±0.066	0.656±0.045
Cox [Matsuo <i>et al.</i> , 2019]		✓		0.637±0.008	0.646±0.021	0.621±0.039	0.680±0.025
SNN-Trans [Shao <i>et al.</i> , 2021]		✓		0.659±0.032	0.647±0.063	0.638±0.022	0.656±0.038
XGBLC [Ma <i>et al.</i> , 2022]		✓		0.681±0.003	0.673±0.006	0.675±0.004	0.680±0.025
GSCNN [Mobadersany <i>et al.</i> , 2018]	✓	✓		0.596±0.014	0.636±0.021	0.617±0.012	0.693±0.031
Pathomic [Chen <i>et al.</i> , 2020]	✓	✓		0.586±0.062	0.657±0.031	0.602±0.014	0.676±0.027
Metric learning [Cheerla and Gevaert, 2019]	✓	✓		0.584±0.012	0.661±0.043	0.613±0.026	0.690±0.011
MultiSurv [Vale-Silva and Rohr, 2021]	✓	✓		0.664±0.012	0.656±0.014	0.626±0.031	0.690±0.015
MCAT [Chen <i>et al.</i> , 2021]	✓	✓		0.672±0.032	0.659±0.031	0.659±0.027	0.649±0.043
HGCN [Hou <i>et al.</i> , 2023]	✓	✓		0.675±0.006	0.671±0.004	0.651±0.008	0.682±0.014
MOTCat [Xu and Chen, 2023]	✓	✓		0.683±0.026	0.673±0.006	0.670±0.038	0.675±0.004
AttnMIL [Chen <i>et al.</i> , 2022]	✓		✓	0.599±0.048	0.609±0.065	0.567±0.010	0.670±0.011
SNN [Chen <i>et al.</i> , 2022]		✓	✓	0.618±0.022	0.624±0.060	0.611±0.047	0.679±0.040
MMF [Chen <i>et al.</i> , 2022]	✓	✓		0.636±0.012	0.674±0.023	0.600±0.057	0.634±0.032
Porpoise [Chen <i>et al.</i> , 2022]	✓	✓	✓	0.636±0.024	0.652±0.042	0.647±0.031	0.675±0.032
FORESEE	✓	✓	✓	0.686±0.008	0.679±0.013	0.672±0.013	0.730±0.002

Table 1: Performance of C-Index (mean±std) on four cancer datasets.

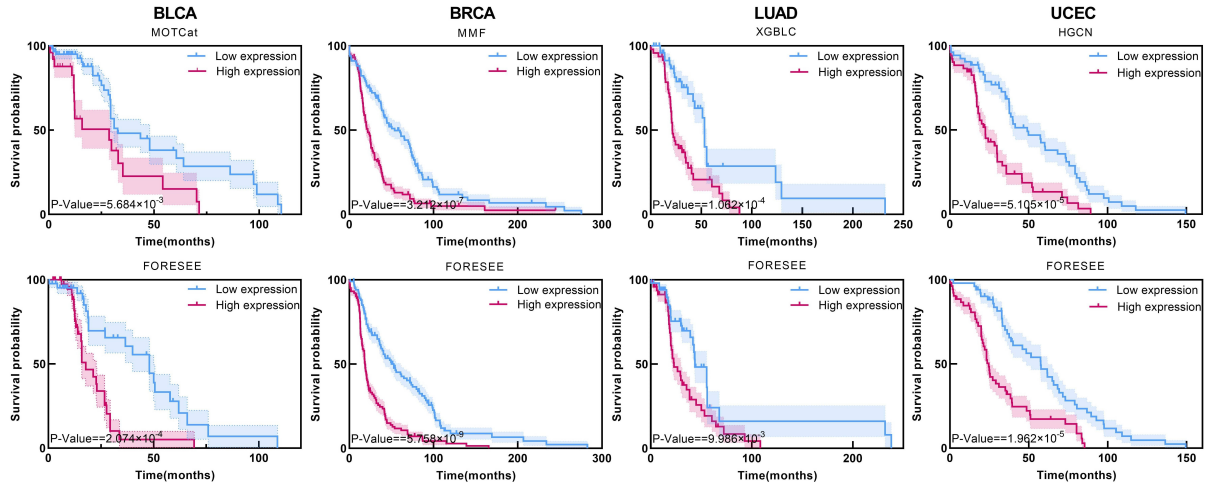


Figure 4: KM analysis compares the performance of state-of-the-art methods with FORESEE tested on four cancer datasets.

Multimodal SOTA v.s. FORESEE: Through a large number of experiments, FORESEE demonstrated an improvement in predictive performance over the SOTA MOTCat by 0.3%, 0.6%, and 3.7% on the BLCA, BRCA, and UCEC datasets, respectively. This indicates that FORESEE enhances the performance of multimodal prediction by incorporating $C\&M$ data, as the expression of $C\&M$ directly signifies the causative factors of cancer. Secondly, the strategy of extracting features from multiple fields of view can effectively assist FORESEE in survival prediction. However, on the UCEC dataset, the XGBLC prediction performance outperformed FORESEE by 0.3%. Of concern is that the method does not generalize to other cancer datasets. Therefore, mining multimodal data for predicting patient survival will be a trend in future research.

Next, we categorized each cancer dataset into high and low expression groups based on the median survival risk predicted by our model. Accurate survival predictions should manifest as a significant divergence in the KM curves between these two groups. Figure 4 illustrates the superior performance of MOTCat, MMF, XGBLC and HGCN on BLCA, BRCA, LUAD and UCEC datasets, respectively, setting the SOTA

benchmarks. The P values of FORESEE in BLCA, BRCA, LUAD and UCEC datasets all surpassed those of the SOTA method, with LUAD patients exhibiting only a slight difference. Nevertheless, the P values of FORESEE across all cancer datasets were consistently below 0.05, affirming the significant value of FORESEE in predicting patient survival.

4.3 Ablation Study

Effect of P_s , P_m and P_l in P modality. To investigate how feature information in large and small fields of view within P modality affects the prognosis of cancer patients, we kept modality data R and $C\&M$ constant while systematically altering the fusion strategy for different fields of view. The results are shown in Table 2. Experiments have found that when P_s , P_m and P_l are utilized individually, P_s can provide features closely related to prognosis for multimodal data. FORESEE experiments in independent R and $C\&M$ modes respectively found that the prediction performance of using multiple fields of view is better than using a single field of view. FORESEE achieved the best prediction performance on the four cancer datasets with the combination of P_s , P_m . However, using only $C\&M$ and multimodal data com-

M	Different Views			BLCA	BRCA	LUAD	UCEC
	P_s	P_m	P_l				
-	✓			0.631±0.035	0.646±0.037	0.644±0.008	0.701±0.021
		✓		0.654±0.027	0.651±0.015	0.635±0.042	0.730±0.006
			✓	0.615±0.016	0.652±0.016	0.598±0.016	0.608±0.013
	✓	✓		0.637±0.021	0.656±0.007	0.661±0.007	0.694±0.011
		✓	✓	0.663±0.003	0.648±0.032	0.657±0.009	0.691±0.006
	✓	✓	✓	0.645±0.031	0.662±0.013	0.658±0.018	0.686±0.004
R	✓			0.681±0.012	0.633±0.028	0.645±0.011	0.687±0.036
		✓		0.654±0.009	0.637±0.013	0.655±0.007	0.679±0.022
			✓	0.664±0.005	0.616±0.016	0.647±0.013	0.663±0.036
	✓	✓		0.674±0.002	0.637±0.012	0.650±0.008	0.693±0.013
		✓	✓	0.631±0.019	0.638±0.024	0.664±0.004	0.675±0.032
	✓	✓	✓	0.683±0.003	0.628±0.041	0.646±0.031	0.661±0.046
C&M	✓			0.677±0.002	0.655±0.028	0.649±0.014	0.688±0.037
		✓		0.649±0.024	0.644±0.018	0.656±0.012	0.671±0.043
			✓	0.662±0.005	0.624±0.026	0.590±0.049	0.635±0.041
	✓	✓		0.671±0.003	0.628±0.035	0.580±0.042	0.608±0.031
		✓	✓	0.664±0.009	0.643±0.013	0.636±0.024	0.673±0.036
	✓	✓	✓	0.651±0.017	0.605±0.035	0.661±0.008	0.646±0.046
R&C&M	✓			0.664±0.003	0.634±0.027	0.568±0.046	0.630±0.039
		✓		0.643±0.018	0.649±0.016	0.616±0.035	0.705±0.002
	✓	✓		0.661±0.007	0.655±0.005	0.660±0.011	0.689±0.025
		✓	✓	0.671±0.002	0.621±0.034	0.629±0.032	0.680±0.014
	✓	✓	✓	0.635±0.016	0.630±0.027	0.621±0.029	0.662±0.043
	✓	✓	✓	0.655±0.012	0.643±0.022	0.665±0.016	0.690±0.008
	✓	✓	0.664±0.007	0.646±0.016	0.678±0.005	0.678±0.026	
	✓	✓	0.649±0.012	0.636±0.025	0.643±0.017	0.650±0.046	
	✓	✓	0.686±0.003	0.679±0.005	0.672±0.008	0.730±0.002	

Table 2: Performance of C-Index (mean) on four cancer datasets.

posed of different independent fields of view predicts poorer survival, possibly because of the lack of complementary modal information to help multimodal data perform survival analysis. The performance of FORESEE in survival analysis using feature information in all fields of view in R and $C&M$ modes is significantly better than other cases where field features are missing. In summary, after a large number of experiments, we found that the fusion of features from different fields of view in pathology images is essential for survival prediction. The survival model FORESEE can obtain survival-related features from the cell level, tissue level, and tumor heterogeneity.

Effect of missing information within modalities. To assess TriMAE’s effectiveness, we conducted ablation experiments to investigate the impact of various MAEs on FORESEE’s prediction performance. Comparison methods included simple MAE [He *et al.*, 2022], ConvMAE [Gao *et al.*, 2022], FCMAE [Woo *et al.*, 2023], DMAE [Wu *et al.*, 2022], PUT [Liu *et al.*, 2022], and MAGE [Li *et al.*, 2023] strategies. Figure 5 illustrates that FORESEE without the use of a MAE is adversely impacted by missing data within the modality, resulting in poor prediction performance. Importantly, TriMAE achieves the best survival prediction results in comparative experiments. This may be attributed to the asymmetric mask design in TriMAE, which allows the model to leverage unmasked portions and masked tokens on different branches to obtain latent feature representations, addressing the issue of information loss in multimodal data. In conclusion, TriMAE is indispensable for multimodal survival prediction.

Effect of HAE. We compare HAE with several advanced molecular feature extraction methods, such as CNN [Gu *et al.*, 2018], LSTM, AutoEncoder [Vahdat and Kautz, 2020], DAE [Du *et al.*, 2016], VAE [Liang *et al.*, 2018], and Transformer [Beltagy *et al.*, 2020] strategies. Figure 6 illustrates

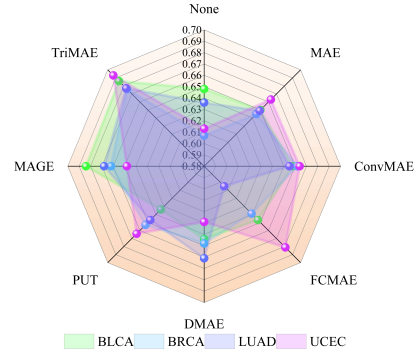


Figure 5: Ablation experiments to evaluate the C-index performance of TriMAE on four cancer datasets in the absence of information within the modality.

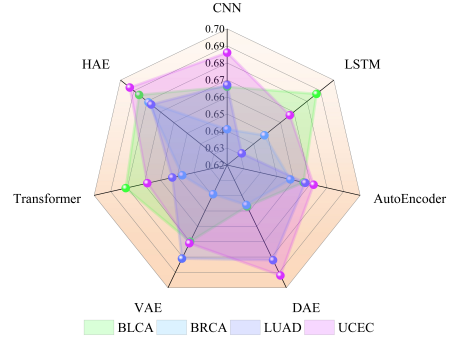


Figure 6: Ablation experiments evaluating the C-index performance of the HAE on four cancer datasets.

the comparative survival prediction results of FORESEE across four cancer datasets. Importantly, HAE achieved optimal results in the BLCA, BRCA, and LUAD datasets. This is attributed to HAE’s CTA module, capable of capturing long-range dependencies among molecular features and acquiring local feature information. HAE’s CNA module introduces global information from molecular data. In summary, HAE exhibits significant advantages in molecular data extraction.

5 Conclusion

This paper proposes a novel end-to-end framework, FORESEE, for robustly predicting patient survival by mining multimodal information. The CFT effectively utilizes features at the cellular level, tissue level, and tumor heterogeneity level, correlating prognosis through a cross-scale feature cross-fusion method. The CTA and CNA modules in HAE can extract features from molecular data at both global and local perspectives. To address missing information within modalities, TriMAE can effectively reconstruct latent feature representations. Extensive experiments on four cancer datasets demonstrate that FORESEE significantly enhances the performance of survival prediction. To assess the impact of different fields of view, TriMAE, and HAE on the prediction performance of FORESEE, ablation experiments show that FORESEE achieves superior prediction performance, validating the necessity of our proposed modules.

References

- [Adewusi and Al-Bedoor, 2001] SA Adewusi and BO Al-Bedoor. Wavelet analysis of vibration signals of an overhang rotor with a propagating transverse crack. *Journal of sound and vibration*, 246(5):777–793, 2001.
- [Beltagy *et al.*, 2020] Iz Beltagy, Matthew E Peters, and Arman Cohan. Longformer: The long-document transformer. *arXiv preprint arXiv:2004.05150*, 2020.
- [Cerami *et al.*, 2012] Ethan Cerami, Jianjiong Gao, Ugur Dogrusoz, Benjamin E Gross, Selcuk Onur Sumer, Bülent Arman Aksoy, Anders Jacobsen, Caitlin J Byrne, Michael L Heuer, Erik Larsson, et al. The cbio cancer genomics portal: an open platform for exploring multidimensional cancer genomics data. *Cancer discovery*, 2(5):401–404, 2012.
- [Chan *et al.*, 2023] Tsai Hor Chan, Fernando Julio Cendra, Lan Ma, Guosheng Yin, and Lequan Yu. Histopathology whole slide image analysis with heterogeneous graph representation learning. In *Proceedings of the IEEE/CVF Conference on Computer Vision and Pattern Recognition*, pages 15661–15670, 2023.
- [Cheerla and Gevaert, 2019] Anika Cheerla and Olivier Gevaert. Deep learning with multimodal representation for pancancer prognosis prediction. *Bioinformatics*, 35(14):i446–i454, 2019.
- [Chen *et al.*, 2020] Richard J Chen, Ming Y Lu, Jingwen Wang, Drew FK Williamson, Scott J Rodig, Neal I Lindeman, and Faisal Mahmood. Pathomic fusion: an integrated framework for fusing histopathology and genomic features for cancer diagnosis and prognosis. *IEEE Transactions on Medical Imaging*, 41(4):757–770, 2020.
- [Chen *et al.*, 2021] Richard J Chen, Ming Y Lu, Wei-Hung Weng, Tiffany Y Chen, Drew FK Williamson, Trevor Manz, Maha Shady, and Faisal Mahmood. Multimodal co-attention transformer for survival prediction in gigapixel whole slide images. In *Proceedings of the IEEE/CVF International Conference on Computer Vision*, pages 4015–4025, 2021.
- [Chen *et al.*, 2022] Richard J Chen, Ming Y Lu, Drew FK Williamson, Tiffany Y Chen, Jana Lipkova, Zahra Noor, Muhammad Shaban, Maha Shady, Mane Williams, Bumjin Joo, et al. Pan-cancer integrative histology-genomic analysis via multimodal deep learning. *Cancer Cell*, 40(8):865–878, 2022.
- [Christensen, 1987] Erik Christensen. Multivariate survival analysis using cox’s regression model. *Hepatology*, 7(6):1346–1358, 1987.
- [Daubechies, 1996] Ingrid Daubechies. Where do wavelets come from? a personal point of view. *Proceedings of the IEEE*, 84(4):510–513, 1996.
- [Du *et al.*, 2016] Bo Du, Wei Xiong, Jia Wu, Lefei Zhang, Liangpei Zhang, and Dacheng Tao. Stacked convolutional denoising auto-encoders for feature representation. *IEEE transactions on cybernetics*, 47(4):1017–1027, 2016.
- [Gao *et al.*, 2020] Jianliang Gao, Tengfei Lyu, Fan Xiong, Jianxin Wang, Weimao Ke, and Zhao Li. Mgnn: A multimodal graph neural network for predicting the survival of cancer patients. In *Proceedings of the 43rd International ACM SIGIR Conference on Research and Development in Information Retrieval*, pages 1697–1700, 2020.
- [Gao *et al.*, 2022] Peng Gao, Teli Ma, Hongsheng Li, Ziyi Lin, Jifeng Dai, and Yu Qiao. Convmae: Masked convolution meets masked autoencoders. *arXiv preprint arXiv:2205.03892*, 2022.
- [Gu *et al.*, 2018] Jiuxiang Gu, Zhenhua Wang, Jason Kuen, Lianyang Ma, Amir Shahroudy, Bing Shuai, Ting Liu, Xingxing Wang, Gang Wang, Jianfei Cai, et al. Recent advances in convolutional neural networks. *Pattern recognition*, 77:354–377, 2018.
- [Gupta *et al.*, 2023] Agrim Gupta, Jiajun Wu, Jia Deng, and Li Fei-Fei. Siamese masked autoencoders. *arXiv preprint arXiv:2305.14344*, 2023.
- [He *et al.*, 2022] Kaiming He, Xinlei Chen, Saining Xie, Yanghao Li, Piotr Dollár, and Ross Girshick. Masked autoencoders are scalable vision learners. In *Proceedings of the IEEE/CVF conference on computer vision and pattern recognition*, pages 16000–16009, 2022.
- [Hou *et al.*, 2023] Wentai Hou, Chengxuan Lin, Lequan Yu, Jing Qin, Rongshan Yu, and Liansheng Wang. Hybrid graph convolutional network with online masked autoencoder for robust multimodal cancer survival prediction. *IEEE Transactions on Medical Imaging*, 2023.
- [Huang *et al.*, 2015] Zhiheng Huang, Wei Xu, and Kai Yu. Bidirectional lstm-crf models for sequence tagging. *arXiv preprint arXiv:1508.01991*, 2015.
- [Kaneko and Harada, 2020] Takuhiro Kaneko and Tatsuya Harada. Noise robust generative adversarial networks. In *Proceedings of the IEEE/CVF conference on computer vision and pattern recognition*, pages 8404–8414, 2020.
- [Kebschull and Zador, 2015] Justus M Kebschull and Anthony M Zador. Sources of pcr-induced distortions in high-throughput sequencing data sets. *Nucleic acids research*, 43(21):e143–e143, 2015.
- [Li *et al.*, 2023] Tianhong Li, Huiwen Chang, Shlok Mishra, Han Zhang, Dina Katabi, and Dilip Krishnan. Mage: Masked generative encoder to unify representation learning and image synthesis. In *Proceedings of the IEEE/CVF Conference on Computer Vision and Pattern Recognition*, pages 2142–2152, 2023.
- [Liang *et al.*, 2018] Dawen Liang, Rahul G Krishnan, Matthew D Hoffman, and Tony Jebara. Variational autoencoders for collaborative filtering. In *Proceedings of the 2018 world wide web conference*, pages 689–698, 2018.
- [Liao *et al.*, 2023] Yuhan Liao, Zhenyu Liu, Yu Zhang, Ping Lu, Lu Wen, and Fuchou Tang. High-throughput and high-sensitivity full-length single-cell rna-seq analysis on third-generation sequencing platform. *Cell Discovery*, 9(1):5, 2023.

- [Liu *et al.*, 2021] Ziyu Liu, Wei Shao, Jie Zhang, Min Zhang, and Kun Huang. Transfer learning via optimal transportation for integrative cancer patient stratification. In *IJCAI*, pages 2760–2766, 2021.
- [Liu *et al.*, 2022] Qiankun Liu, Zhentao Tan, Dongdong Chen, Qi Chu, Xiyang Dai, Yinpeng Chen, Mengchen Liu, Lu Yuan, and Nenghai Yu. Reduce information loss in transformers for pluralistic image inpainting. In *Proceedings of the IEEE/CVF Conference on Computer Vision and Pattern Recognition*, pages 11347–11357, 2022.
- [Lu *et al.*, 2021] Ming Y Lu, Drew FK Williamson, Tiffany Y Chen, Richard J Chen, Matteo Barbieri, and Faisal Mahmood. Data-efficient and weakly supervised computational pathology on whole-slide images. *Nature biomedical engineering*, 5(6):555–570, 2021.
- [Ma *et al.*, 2022] Baoshan Ma, Ge Yan, Bingjie Chai, and Xiaoyu Hou. Xgblc: an improved survival prediction model based on xgboost. *Bioinformatics*, 38(2):410–418, 2022.
- [Matsuo *et al.*, 2019] Koji Matsuo, Sanjay Purushotham, Bo Jiang, Rachel S Mandelbaum, Tsuyoshi Takiuchi, Yan Liu, and Lynda D Roman. Survival outcome prediction in cervical cancer: Cox models vs deep-learning model. *American journal of obstetrics and gynecology*, 220(4):381–e1, 2019.
- [Mobadersany *et al.*, 2018] Pooya Mobadersany, Safoora Yousefi, Mohamed Amgad, David A Gutman, Jill S Barnholtz-Sloan, José E Velázquez Vega, Daniel J Brat, and Lee AD Cooper. Predicting cancer outcomes from histology and genomics using convolutional networks. *Proceedings of the National Academy of Sciences*, 115(13):E2970–E2979, 2018.
- [Riasatian *et al.*, 2021] Abtin Riasatian, Morteza Babaie, Danial Maleki, Shivam Kalra, Mojtaba Valipour, Sobhan Hemati, Mani Zaveri, Amir Safarpour, Sobhan Shafiei, Mehdi Afshari, et al. Fine-tuning and training of densenet for histopathology image representation using tcga diagnostic slides. *Medical Image Analysis*, 70:102032, 2021.
- [Shao *et al.*, 2021] Zhuchen Shao, Hao Bian, Yang Chen, Yifeng Wang, Jian Zhang, Xiangyang Ji, et al. Transmil: Transformer based correlated multiple instance learning for whole slide image classification. *Advances in neural information processing systems*, 34:2136–2147, 2021.
- [Shi *et al.*, 2023] Jiangbo Shi, Lufei Tang, Zeyu Gao, Yang Li, Chunbao Wang, Tieliang Gong, Chen Li, and Huazhu Fu. Mg-trans: Multi-scale graph transformer with information bottleneck for whole slide image classification. *IEEE Transactions on Medical Imaging*, 2023.
- [Vahdat and Kautz, 2020] Arash Vahdat and Jan Kautz. Nvae: A deep hierarchical variational autoencoder. *Advances in neural information processing systems*, 33:19667–19679, 2020.
- [Vale-Silva and Rohr, 2021] Luís A Vale-Silva and Karl Rohr. Long-term cancer survival prediction using multimodal deep learning. *Scientific Reports*, 11(1):13505, 2021.
- [Wang *et al.*, 2021] Zhiqin Wang, Ruiqing Li, Minghui Wang, and Ao Li. Gpdbn: deep bilinear network integrating both genomic data and pathological images for breast cancer prognosis prediction. *Bioinformatics*, 37(18):2963–2970, 2021.
- [Wang *et al.*, 2022] Xuan Wang, Harrison G Zhang, Xin Xiong, Chuan Hong, Griffin M Weber, Gabriel A Brat, Clara-Lea Bonzel, Yuan Luo, Rui Duan, Nathan P Palmer, et al. Survmaximin: robust federated approach to transporting survival risk prediction models. *Journal of biomedical informatics*, 134:104176, 2022.
- [Woo *et al.*, 2023] Sanghyun Woo, Shoubhik Debnath, Ronghang Hu, Xinlei Chen, Zhuang Liu, In So Kweon, and Saining Xie. Convnext v2: Co-designing and scaling convnets with masked autoencoders. In *Proceedings of the IEEE/CVF Conference on Computer Vision and Pattern Recognition*, pages 16133–16142, 2023.
- [Wu *et al.*, 2022] QuanLin Wu, Hang Ye, Yuntian Gu, Huishuai Zhang, Liwei Wang, and Di He. Denoising masked autoencoders help robust classification. In *The Eleventh International Conference on Learning Representations*, 2022.
- [Xu and Chen, 2023] Yingxue Xu and Hao Chen. Multimodal optimal transport-based co-attention transformer with global structure consistency for survival prediction. *arXiv preprint arXiv:2306.08330*, 2023.
- [Yao *et al.*, 2020] Jiawen Yao, Xinliang Zhu, Jitendra Jonnagaddala, Nicholas Hawkins, and Junzhou Huang. Whole slide images based cancer survival prediction using attention guided deep multiple instance learning networks. *Medical Image Analysis*, 65:101789, 2020.
- [Zhang and Wu, 2022] Donglin Zhang and Xiao-Jun Wu. Robust and discrete matrix factorization hashing for cross-modal retrieval. *Pattern Recognition*, 122:108343, 2022.
- [Zhang *et al.*, 2017] Hongyi Zhang, Moustapha Cisse, Yann N Dauphin, and David Lopez-Paz. mixup: Beyond empirical risk minimization. *arXiv preprint arXiv:1710.09412*, 2017.
- [Zhang *et al.*, 2022] Hongrun Zhang, Yanda Meng, Yitian Zhao, Yihong Qiao, Xiaoyun Yang, Sarah E Coupland, and Yalin Zheng. Dtf-d-mil: Double-tier feature distillation multiple instance learning for histopathology whole slide image classification. In *Proceedings of the IEEE/CVF Conference on Computer Vision and Pattern Recognition*, pages 18802–18812, 2022.
- [Zhao *et al.*, 2023] Weiqin Zhao, Shujun Wang, Maximus Yeung, Tianye Niu, and Lequan Yu. Mulgt: Multi-task graph-transformer with task-aware knowledge injection and domain knowledge-driven pooling for whole slide image analysis. *arXiv preprint arXiv:2302.10574*, 2023.